Supplementary Information

Dual Regulatory Roles of CO_2 on Molecular Sulfur Dissolution in Sour Components of High-sulfur Natural Gas: Insight from Molecular Dynamics Simulations

Shuangli Yue, [a, b] Nong Li, [a] Li Wang [a, *], Ying Wan, [a] Chengxin He, [c] Li Zhang, [b,*] Mingli Yang [b]

[a] Research Institute of Exploration and Development, PetroChina Southwest Oil and Gasfield Company, Chengdu 610213, China

[b] Institute of Atomic and Molecular Physics, Sichuan University, Chengdu 610065, China

[c] Suzhou Laboratory, Suzhou 215123, China

[*] Corresponding authors
E-mail addresses: wangli2022222@sina.com (Li Wang), lizhang@scu.edu.cn (Li Zhang)

1. CO_2–H_2S Association Model

An association model can be suggested to elucidate the intermolecular interaction in the system. It is assumed that CO_2 reversibly associates with H_2S to form a complex of $H_2S(CO_2)_n$, represented by

$$H_2S + nCO_2 \leftrightharpoons H_2S \cdot (CO_2)_n \tag{1}$$

where n denotes the coordination number of CO_2 in the complex. The equilibrium constant K is defined as

$$K = \frac{H_2S \cdot (CO_2)_n}{H_2S \cdot {CO_2}^n} \tag{2}$$

The solubility (S) in the mixed system is then expressed as

$$S = S_0 \times [H_2S] + S_1 \times CO_2 \tag{3}$$

where S_0 is the solubility of elemental sulfur in pure H_2S, which is 13.93 mmol/mol. The solubility of S_8 in pure CO_2 was also calculated and is referred to as S_1, with a value of 1.84 mmol/mol. Based on this association model, the coordination number n was determined by fitting the simulation S_8 solubility data using a nonlinear least-squares method, in which n was optimized by minimizing the squared deviation between the model prediction and the simulation results. The fitted value n = 0.62 indicates that although CO_2 does not form a strong or stable complex with H_2S, a weak local association still exists. CO_2 molecules partially occupy the solvation environment around H_2S, thereby weakening its solvation interaction with S_8 and reducing S_8 solubility. This result indicates that, as CO_2 is gradually introduced into a pure H_2S system, the solubility of S_8 does not follow a simple additive trend of the two solvents, instead, the interactions between CO_2 and H_2S must be fully considered. Furthermore, this finding is consistent with the corrected PRDF analysis in Fig. 4, where increasing CO_2 concentration leads to a notable decline in the local density of S_8–H_2S pairs, while enhancing the presence of H_2S–CO_2 and S_8–CO_2 pairs. These observations support the assumptions of the association model at the microscopic level

2. Force-Field Validation

To evaluate the impact of force-field models and combining-rule choices on the calculated results, the H_2S–CO_2 system was taken as a representative case. Comparative tests were performed using coarse-grained [1,2] and all-atom [3,4] force fields, in combination with the Lorentz–Berthelot (LB) mixing rule and the geometric mixing rule. The corresponding force-field parameters are provided in Tables S1 and S2. In the Lorentz-Berthelot mixing rule, the cross Lennard–Jones parameters are defined as

$$\epsilon_{ij} = \sqrt{\epsilon_i \epsilon_j} \tag{4}$$

$$\sigma_{ij} = \frac{1}{2}(\sigma_i + \sigma_j) \tag{5}$$

whereas in the geometric mixing rule they are given by,

$$\epsilon_{ij} = \sqrt{\epsilon_i \epsilon_j} \tag{6}$$

$$\sigma_{ij} = \sqrt{\sigma_i \sigma_j} \tag{7}$$

Consistent trends are observed for different combining rules and force field models, with all deviations within acceptable statistical uncertainty, as illustrated in Fig. S4. Such benchmark calculations indicate that the computational strategies in this work are adequate to produce reliable results for addressing the solubility evolution mechanism of elementary sulfur in the mixed gases.

Table S1 The coarse-grained force-field parameters used in this work [1,2]

	ε (kcal/mol)	σ (Å)	charge
H_2S	0.563	3.667	0
CO_2	0.459	3.627	0
CH_4	0.294	3.730	0

Table S2 The all-atom force-field parameters for CO_2 and H_2S used in this work [3,4]

Aom pair	ε (kcal/mol)	σ (Å)	charge
S	0.497	3.720	-0.2480
H	0.008	0.980	0.1240
C	0.056	2.800	0.6512
O	0.160	3.028	-0.3256
Bond coeff	K (kcal/mol Å^2)		r_0 (Å)
S-H	95.805		1.365
C-O	1008.963		1.162
Angle coeff	K (kcal/mol)		θ_0
H-S-H	62.050		91.500
O-C-O	54.003		180.000

Table S3 Comparison of density between MD simulation and PR-EOS at 393.15 K and 40 MPa under different CO_2 counts in H_2S–CO_2 binary solvent systems.

Numbers of S_8	Numbers of H_2S	Numbers of CO_2	ρ (g/m^3)		$\Delta\rho$ (g/m^3)
			MD simulation	PR-EOS	
1,000	20,000	0	0.836	0.913	0.077
		500	0.834	0.910	0.076
		1,000	0.830	0.908	0.078
		1,500	0.829	0.905	0.076
		2,000	0.825	0.902	0.077
		2,500	0.822	0.900	0.078
		5,000	0.812	0.887	0.075
		10,000	0.793	0.866	0.073
		15,000	0.780	0.846	0.066
		20,000	0.770	0.831	0.061
		25,000	0.762	0.817	0.055
		30,000	0.756	0.806	0.050
		35,000	0.751	0.796	0.045
		40,000	0.746	0.787	0.041
		45,000	0.744	0.780	0.036
		50,000	0.741	0.774	0.033

Table S4 Comparison of density between MD simulation and PR-EOS at 393.15 K and 40 MPa under different CO_2 counts in H_2S–CH_4–CO_2 ternary solvent systems (1:4).

Numbers of S_8	Numbers of H_2S	Numbers of CH_4	Numbers of CO_2	ρ (g/m^3)		$\Delta\rho$ (g/m^3)
				MD simulation	PR-EOS	
500	10,000	40,000	0	0.263	0.286	0.023
			1,000	0.269	0.291	0.022
			2,000	0.275	0.298	0.023
			3,000	0.281	0.304	0.023
			4,000	0.288	0.310	0.022
			5,000	0.293	0.315	0.022
			10,000	0.319	0.341	0.022
			15,000	0.341	0.364	0.023
			20,000	0.361	0.384	0.023
			25,000	0.379	0.401	0.022
			30,000	0.395	0.417	0.022
			35,000	0.410	0.431	0.021
			40,000	0.423	0.444	0.021
			45,000	0.435	0.455	0.020
			50,000	0.446	0.465	0.019

Table S5 Comparison of density between MD simulation and PR-EOS at 393.15 K and 40 MPa under different CO_2 counts in H_2S–CH_4–CO_2 ternary solvent systems (1:6).

Numbers of S_8	Numbers of H_2S	Numbers of CH_4	Numbers of CO_2	ρ (g/m^3)		$\Delta\rho$ (g/m^3)
				MD simulation	PR-EOS	
500	10,000	60,000	0	0.237	0.255	0.018
			5,000	0.260	0.278	0.018
			10,000	0.279	0.298	0.019
			15,000	0.298	0.317	0.019
			20,000	0.315	0.334	0.019
			25,000	0.331	0.349	0.018
			30,000	0.345	0.363	0.018
			35,000	0.358	0.376	0.018
			40,000	0.370	0.388	0.018
			45,000	0.381	0.399	0.018
			50,000	0.392	0.410	0.018

Table S6 Solubility of S_8 and number of aggregated S_8 molecules under different CO_2 counts in H_2S–CO_2 binary solvent systems. N = number of independent MD trajectories used for uncertainty estimation.

Numbers of S_8	Numbers of H_2S	Numbers of CO_2	S (mmol/mol)	Number of aggregated S_8 molecules	N
1,000	20,000	0	13.63±0.093	727.40±1.860	3
		500	12.69±0.083	739.86±1.702	3
		1,000	12.34±0.003	740.86±0.063	3
		1,500	12.18±0.170	738.13±3.655	3
		2,000	11.86±0.052	739.08±1.144	3
		2,500	10.85±0.022	755.88±0.495	3
		5,000	7.98±0.155	800.63±3.875	3
		10,000	5.90±0.125	823.15±3.750	3
		15,000	3.86±0.055	865.08±1.925	3
		20,000	3.36±0.010	865.60±0.400	3
		25,000	2.91±0.045	869.28±2.025	3
		30,000	2.75±0.005	862.75±0.250	3
		35,000	2.47±0.070	864.15±3.850	3
		40,000	2.27±0.015	864.10±0.900	3
		45,000	2.02±0.050	868.70±3.250	3
		50,000	1.90±0.010	867.00±0.700	3

Table S7 Solubility of S_8 and number of aggregated S_8 molecules under different CO_2 counts in H_2S–CH_4–CO_2 ternary solvent systems (1:4). N = number of independent MD trajectories used for uncertainty estimation.

Numbers of S_8	Numbers of H_2S	Numbers of CH_4	Numbers of CO_2	S (mmol/mol)	Number of aggregated S_8 molecules	N
500	10,000	40,000	0	0.33±0.007	483.50±0.350	3
			1,000	0.31±0.009	484.04±0.459	3
			2,000	0.32±0.017	483.41±0.884	3
			3,000	0.31±0.012	483.52±0.636	3
			4,000	0.32±0.005	482.56±0.270	3
			5,000	0.32±0.013	482.46±0.715	3
			10,000	0.32±0.002	480.80±0.120	3
			15,000	0.33±0.006	478.88±0.390	3
			20,000	0.33±0.007	476.62±0.490	3
			25,000	0.35±0.003	473.68±0.225	3
			30,000	0.35±0.005	471.84±0.400	3
			35,000	0.36±0.013	469.15±1.105	3
			40,000	0.43±0.012	461.48±1.080	3
			45,000	0.44±0.016	458.30±1.520	3
			50,000	0.45±0.012	455.30±1.200	3

Table S8 Solubility of S_8 and number of aggregated S_8 molecules under different CO_2 counts in H_2S–CH_4–CO_2 ternary solvent systems (1:6). N = number of independent MD trajectories used for uncertainty estimation.

Numbers of S_8	Numbers of H_2S	Numbers of CH_4	Numbers of CO_2	S (mmol/mol)	Number of aggregated S_8 molecules	N
500	10,000	40,000	0	0.233±0.003	483.69±0.210	3
			5,000	0.235±0.011	482.38±0.825	3
			10,000	0.252±0.012	479.84±0.960	3
			15,000	0.267±0.001	477.31±0.085	3
			20,000	0.269±0.008	475.79±0.720	3
			25,000	0.281±0.005	473.31±0.475	3
			30,000	0.299±0.014	470.10±1.400	3
			35,000	0.309±0.002	467.56±0.210	3
			40,000	0.315±0.008	465.35±0.880	3
			45,000	0.346±0.002	460.21±0.230	3
			50,000	0.388±0.008	453.44±0.960	3

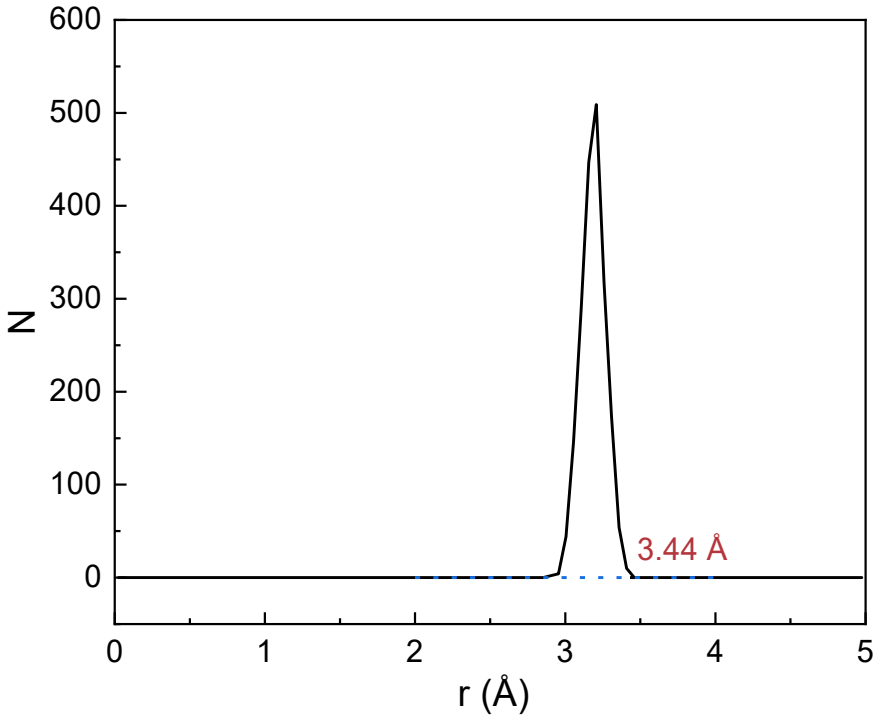

Fig. S1 The shortest intermolecular distances between neighboring S_8 molecules in the pure S_8 system

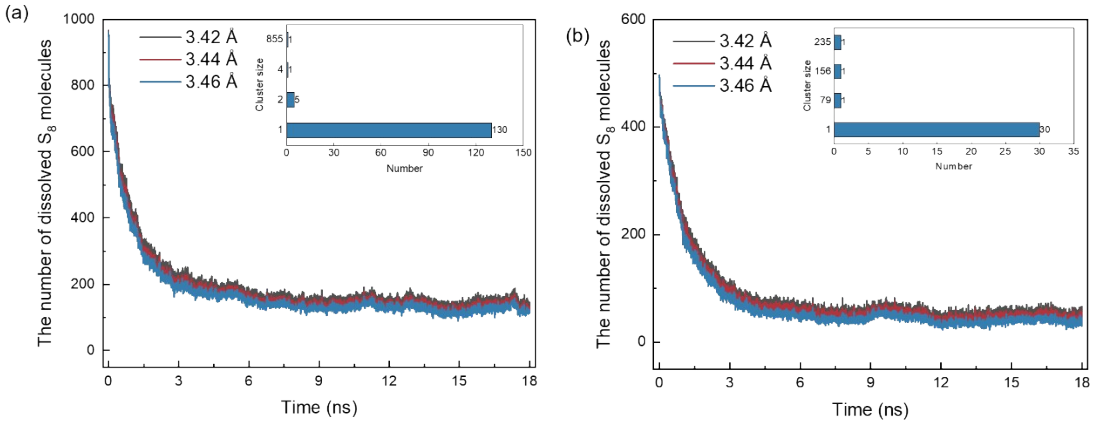

Fig. S2 Sensitivity of S_8 cluster identification to the cutoff distance and the corresponding cluster-size distributions. (a) H_2S–CO_2 system and (b) H_2S–CO_2–CH_4 system, each containing 40,000 CO_2 molecules.

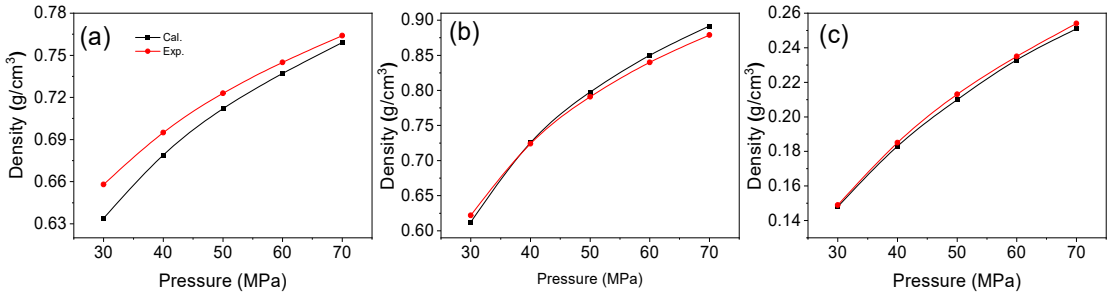

Fig. S3 Comparison between simulated densities and experimental data [5-7]: (a) H_2S, (b) CO_2, and (c) CH_4.

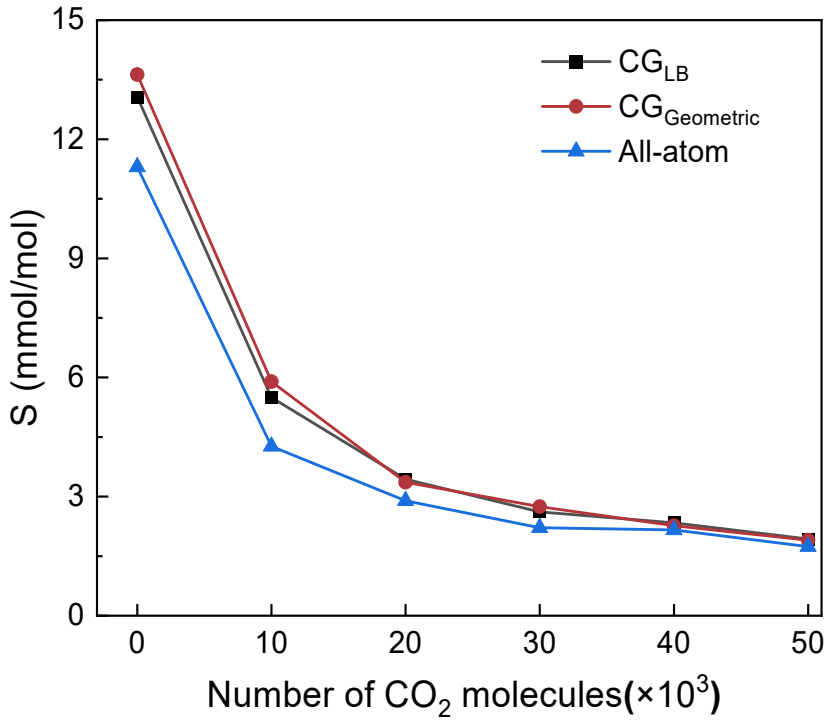

Fig. S4 Solubility of S_8 (S, mmol/mol) in the binary H_2S–CO_2 system as a function of the number of CO_2 molecules, calculated using a coarse-grained force field with the Lorentz–Berthelot (CG_{LB}) mixing rule, a coarse-grained force field with the geometric mixing rule ($CG_{Geometric}$), and an all-atom force field. All calculations were performed at T = 393 K and P = 40 MPa.

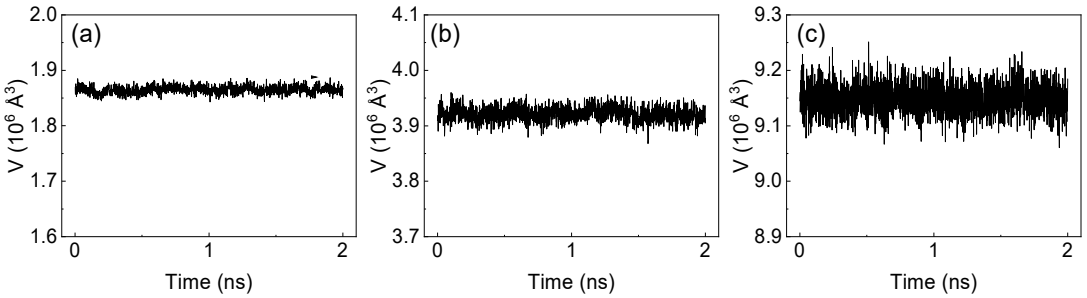

Fig. S5 Time evolution of the simulation cell volume during the 2 ns production stage for (a) unary H_2S, (b) binary H_2S–CO_2, and (c) ternary H_2S–CO_2–CH_4 systems at 393 K and 40 MPa.

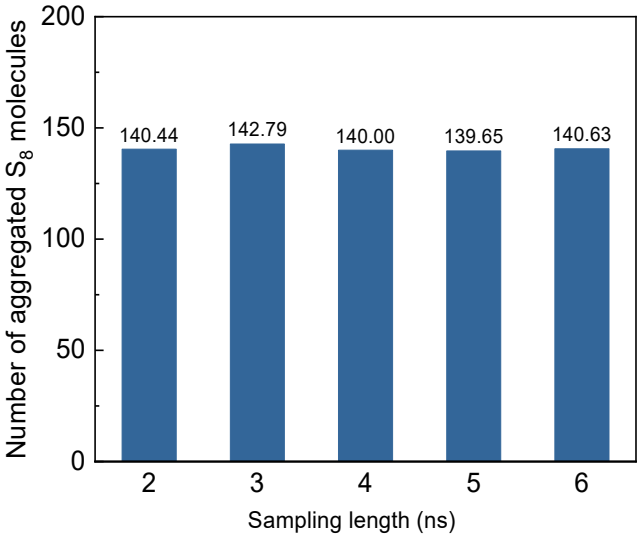

Fig. S6 Number of S_8 clusters obtained using different sampling durations.

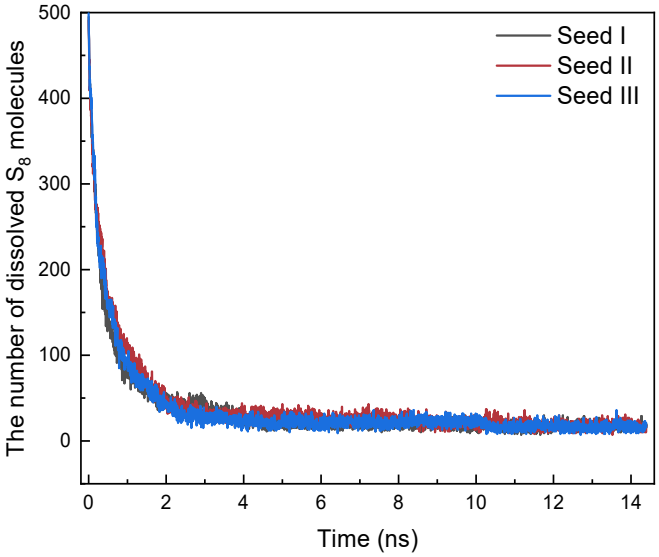

Fig. S7 Temporal evolution of S_8 aggregate population during the production run, showing stable fluctuations.

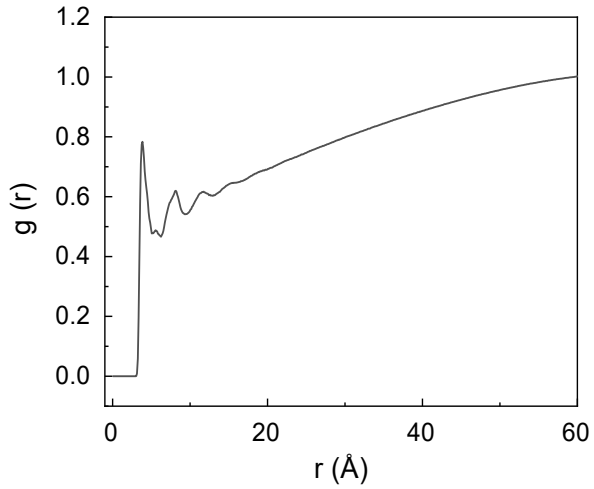

Fig. S8 PRDF between S_8 and H_2S in the binary H_2S-CO_2 system.

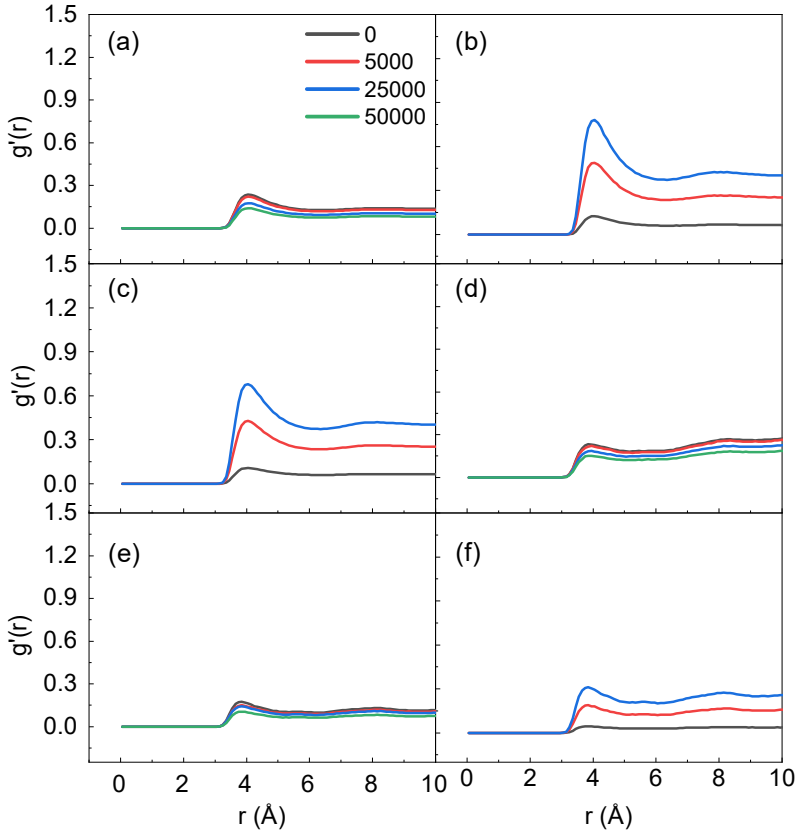

Fig. S9 Corrected pair radial distribution functions g′(r) in the H_2S/CH_4 = 1:6 system for different CO_2 concentrations (0, 5,000; 25,000; 50,000 molecules), showing the spatial distribution evolution of CH_4–H_2S (a), CH_4–CO_2 (b), H_2S–CO_2 (c), S_8–CH_4 (d), S_8–H_2S (e), and S_8–CO_2 (f) molecular pairs.

Supplementary References

1. G. Galliero, C. Nieto-Draghi, C. Boned, J. B. Avalos, A. D. Mackie, A. Baylaucq and F. Montel, *Ind. Eng. Chem. Res.*, 2007, **46**, 5238-5244.
2. M. G. Martin and J. I. Siepmann, *J. Phys. Chem. B*, 1998, **102**, 2569-2577.
3. R. Hens and T. J. H. Vlugt, *J. Chem. Eng. Data*, 2018, **63**, 1096–1102.
4. R. T. Cygan, V. N. Romanov and E. M. Myshakin, *J. Phys. Chem. C*, 2012, 116, 13079–13091.
5. E. W. Lemmon and R. Span, *J. Chem. Eng. Data*, 2006, **51**, 785-850.
6. A. Laesecke and C. D. Muzny, *J. Phys. Chem.*, 2017, **46**, 013107.
7. U. Setzmann and W. Wagner, *J. Phys. Chem.*, 1991, **20**, 1061-1155.